Characteristics of edge pedestals in LHW and NBI heated H-mode plasmas on EAST

2016 Nucl. Fusion 56 106003

(http://iopscience.iop.org/0029-5515/56/10/106003)

OPEN ACCESS
IOP Publishing | International Atomic Energy Agency
Nuclear Fusion
Nucl. Fusion **56** (2016) 106003 (8pp)
doi:10.1088/0029-5515/56/10/106003

Characteristics of edge pedestals in LHW and NBI heated H-mode plasmas on EAST

Q. Zang[1,a], T. Wang[1], Y. Liang[1,2], Y. Sun[1], H. Chen[1], S. Xiao[1], X. Han[1], A. Hu[1], C. Hsieh[3], H. Zhou[1], J. Zhao[1], T. Zhang[1], X. Gong[1], L. Hu[1], F. Liu[1], C.Hu[1], X. Gao[1], B. Wan[1] and the EAST Team

[1] Institute of Plasma Physics, Chinese Academy of Sciences, PO Box 1126, Hefei, Anhui 230031, People's Republic of China
[2] Forschungszentrum Juelich GmbH, 52425 Juelich, Germany
[3] General Atomics, San Diego, CA 092186-5608, USA

E-mail: zangq@ipp.ac.cn

Received 6 February 2016, revised 21 May 2016
Accepted for publication 14 June 2016
Published 28 July 2016

Abstract

By using the recently developed Thomson scattering diagnostic, the pedestal structure of the H-mode with neutral beam injection (NBI) or/and lower hybrid wave (LHW) heating on EAST (Experimental Advanced Superconducting Tokamak) is analyzed in detail. We find that a higher ratio of the power of the NBI to the total power of the NBI and the lower hybrid wave (LHW) will produce a large and regular different edge-localized mode (ELM), and a lower ratio will produce a small and irregular ELM. The experiments show that the mean pedestal width has good correlation with $\beta_{\mathrm{p,ped}}^{0.5}$, The pedestal width appears to be wider than that on other similar machines, which could be due to lithium coating. However, it is difficult to draw any conclusion of correlation between ρ^* and the pedestal width for limited ρ^* variation and scattered distribution. It is also found that $T_e/\nabla T_e$ is ~2 cm, which is the same as the AUG (ASDEX Upgrade), DIII-D and JET (Joint European Torus) results.

Keywords: EAST tokamak, Thomson scattering diagnostic, pedestal structure

(Some figures may appear in colour only in the online journal)

1. Introduction

The high confinement regime H-mode is one of the most promising scenarios for tokamak operation. The pedestal is a remarkable feature of H-mode confinement in tokamak edge plasmas, and is assumed to be associated with high performance and achievable central temperature. Since the first H-mode was found in ASDEX [1], different types of H-mode plasma have been achieved in different tokamaks [2–6]. Recently, with the increase of the power of the heating system of EAST (Experimental Advanced Superconducting Tokamak), a variety of H-mode regimes have been achieved with the different edge-localized mode (ELM). Generally, almost all EAST H-mode discharges appear under lithium wall coating conditioning, type III ELMs can be obtained in lower single null (LSN) or double null (DN) configurations with a lower hybrid current drive (LHCD), while type I ELMs need to combine with LHCD and other auxiliary heating system. Although, the first type I ELM H-mode was achieved on EAST in 2012 with an LHCD plus ion cyclotron resonance heating (ICRH) [7], most type I ELMs are currently obtained mainly by neutral beam injection (NBI) heating in an LSN configuration. The pedestal is a remarkable feature of the H-mode; it is located in the intermediate region between the hot plasma and the cold unconfined region, and it is believed to cause almost all fusion relevant parameters (T, n and τ_{E}) to increase significantly. With the help of the recently developed Thomson scattering (TS) diagnostic and other edge diagnostics, the study of the pedestal structure has recently

[a] Author to whom correspondence should be addressed.

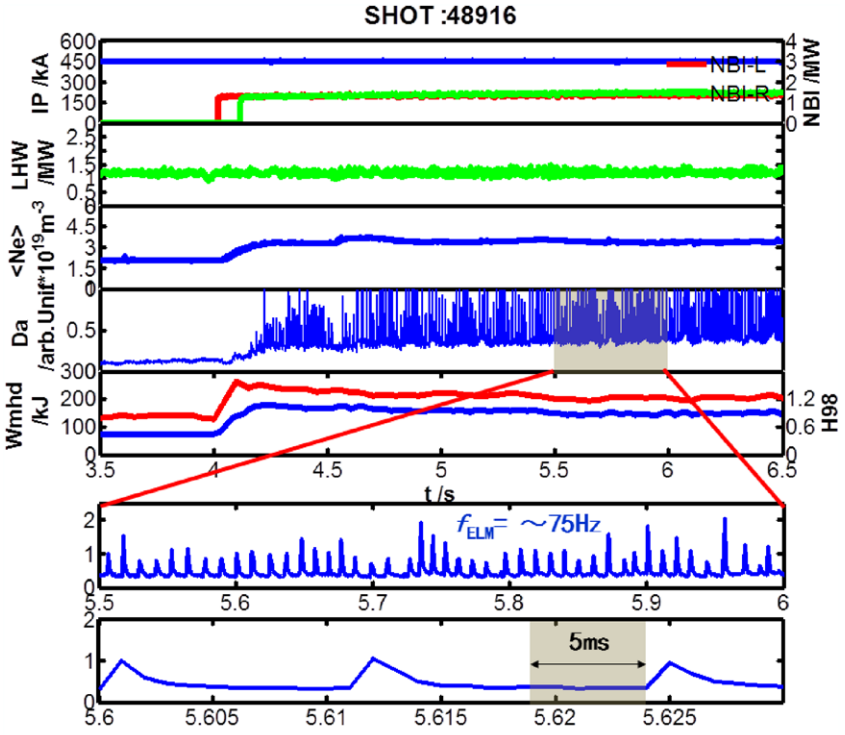

(a)

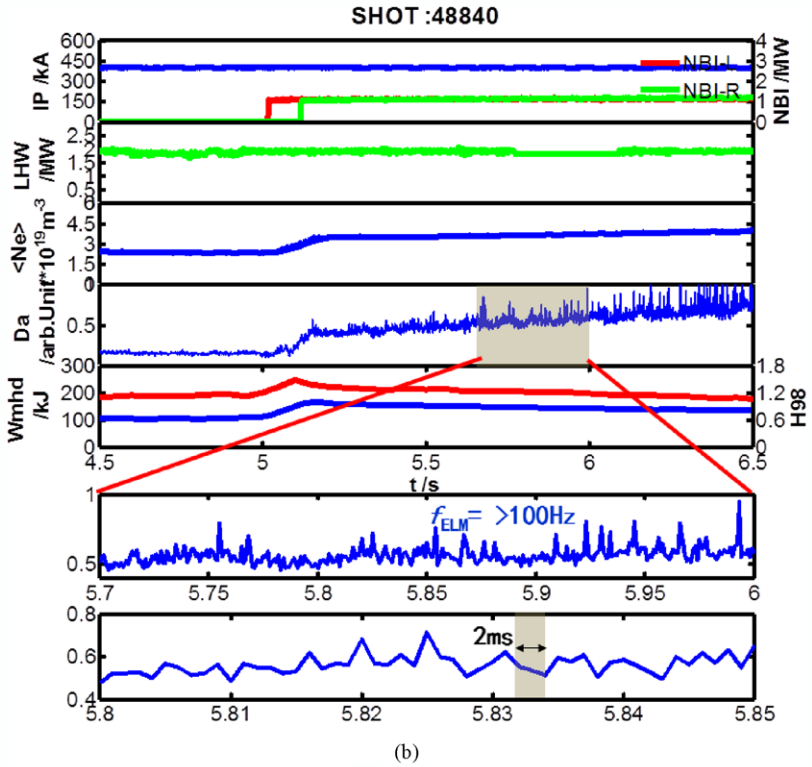

(b)

Figure 1. Typical NBI and LHW injecting H-mode discharges on EAST. (*a*) $I_p = 450$ kA, $\langle n_e \rangle = \sim 3 \times 10^{19}$ m^{-3}, $P_{NBI}/(P_{NBI} + P_{LHW}) > 0.67$, type I-like regular ELMs; (*b*) $I_p = 410$ kA, $\langle n_e \rangle = \sim 3 \times 10^{19}$ m^{-3}, $P_{NBI}/(P_{NBI} + P_{LHW}) < 0.55$, type III-like irregular ELMs. NBI-L and NBI-R mean the more tangential left (LT) and the less tangential right (RT) sources, respectively [10].

become possible on EAST. The pedestal structures of type I ELM and type III ELM H-mode discharges, which are by far the most common two high confinement regimes on EAST, are mainly discussed in this paper. This is the first systematic study of the pedestal structure on EAST, and three pedestal characteristics—the value at the transition to the core plasma (pedestal height), the extent of the pedestal region (pedestal width) and the gradient of the pedestal—are analyzed with

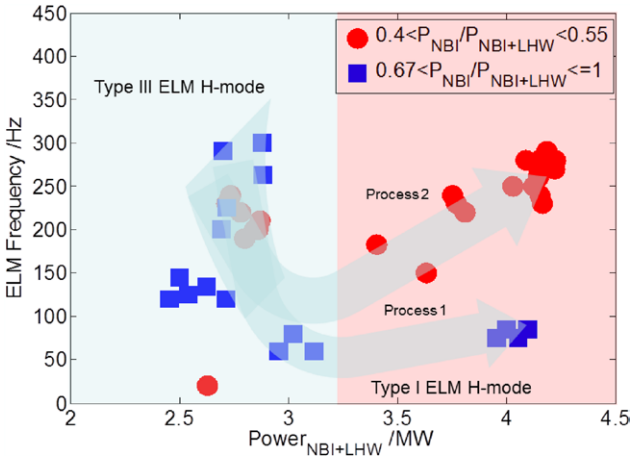

Figure 2. Dependence of the frequency of the H-mode discharges on the power of injection.

other plasma properties, some results of these analyses are compared with various theories, and the major influences on the pedestal structure are discussed.

2. Experimental characterization of the EAST H-mode pedestal

EAST is a fully superconducting tokamak with upper and lower divertor geometry, which can accommodate both SN (including LSN and upper single null, USN) and DN configurations. It has a major radius $R = 1.7$–1.9 m and a minor radius $a = 0.4$–0.45 m, with triangularity $\delta = 0.4$–0.7, elongation κ up to 1.9, and the designed maximum plasma current I_p and the toroidal field B_t are up to 1 MA, and 3.5 T, respectively [8]. Before the 2010 campaign, the plasma facing components (PFCs) were SiC-coated doped graphite tiles in EAST, while in the 2012 campaign, the LFS (low-field side) and HFS (high-field side) tiles were changed to molybdenum; both the lower and upper divertor targets remained as graphite. In the 2014 and 2015 campaigns, in order to try ITER-like operation, the upper divertor targets were changed to tungsten. Since 2011 the first H-mode was achieved on EAST with LHCD, ICRH and NBI were gradually applied, and they have proved to be successful in achieving high performance.

Figure 1 gives two kinds of ELMy H-mode produced by LHCD + NBI on EAST. Both shots have similar plasma background parameters, and on NBI, $D\alpha$ signals decrease and H-factor values increase, which means that they enter into H-mode immediately after NBI. The figure shows that, even though the total power of figure 1(b) is a litter larger than figure 1(a), when the ratio of the power of NBI to the total power of NBI and LHW (RNT) is higher than 67%, the plasma has a type I-like regular ELM (figure 1(a)), and when the RNT is lower than 55%, the plasma has a type III-like irregular ELM (figure 1(b)). This phenomenon is expected to be explained by the effect of the LHW, which strong mitigates the ELMs [9]. All of the power above refers to absorbed power.

In fact, when the total power is larger than 2 MW, the plasma begins to enter the H-mode, whether as the emergence of regular ELMs or irregular ELMs. But when the RNT is higher than 67% (higher RNT), the frequency of the ELMs increases slowly with increasing the total power, which is similar to the type I ELMy H-mode, while when the RNT is lower than 55% (lower RNT), the LHW begin to dominates the heating, and the frequency of ELMs increases dramatically with increasing of total power, which is similar to the type III ELMy H-mode (figure 2). Although there are some differences, the confinement of both regimes are improved during the H-mode phase for the plasma energy (W_{mhd}) and H-factor increase at the same time.

All the data in this paper are selected in a pre-ELM time window, which is before the ELM crash. Considering the temporal resolution of the TS diagnostic and evaluation of ELMs, the intervals are determined to be ~5 ms and ~2 ms for regular and irregular ELM discharges, respectively. All pulses are chosen to be located in the right shaded region of figure 2 with high power injection.

3. Diagnostic and data analysis method

3.1. Diagnostic

Recently, an upgraded core Thomson system has been developed on EAST for full up-half space measurement, when more than ten channels are added in the former system [11]. Figure 3(a) is a typical H-mode plasma flux; the elongation equals 1.7 and the red squares show the positions corresponding to each channel of the EAST Thomson system. There are up to 40 available points, and the detectable area is extended to −35cm to +65cm, which covers the full pedestal and core area from 0 to 1a (a is the minor radius) in almost all discharges. In particular, a compact fiber bound, including five independent channels (height × width = 2.3 mm × 1.6 mm), is designed for pedestal measurement. Considering the magnification (~1/6) of the collective lens, the pedestal spatial resolution is about 7 mm in the minor radius, which means that at least five points can be used to describe the EAST pedestal.

On the other hand, a high power and high frequency Nd YAG laser (1064 nm/3 J/50 Hz) is involved, and it is important to improve the temporal resolution of the upgraded system.

In addition, a new polychromator has been designed for low temperature and low density, which is an upgrade of the DIII-D design. The optical and mechanical systems have been redesigned for higher quality of imaging, and a cooling system is involved in the new circuit for the polychromator to work steadily without the influence of environmental temperature [12].

For the improvement of the capabilities of the system and the calibration techniques, the error of the electron temperature (T_e) is estimated to be below 10% and the electron density (n_e) error is less than 15%.

3.2. Pedestal data and method of pedestal analysis

The coordinates of measured data are usually expressed directly by the machine coordinates: R (radial coordinate), z (vertical coordinate) and Φ (toroidal angle). In order to compare different diagnostics data from different locations, and

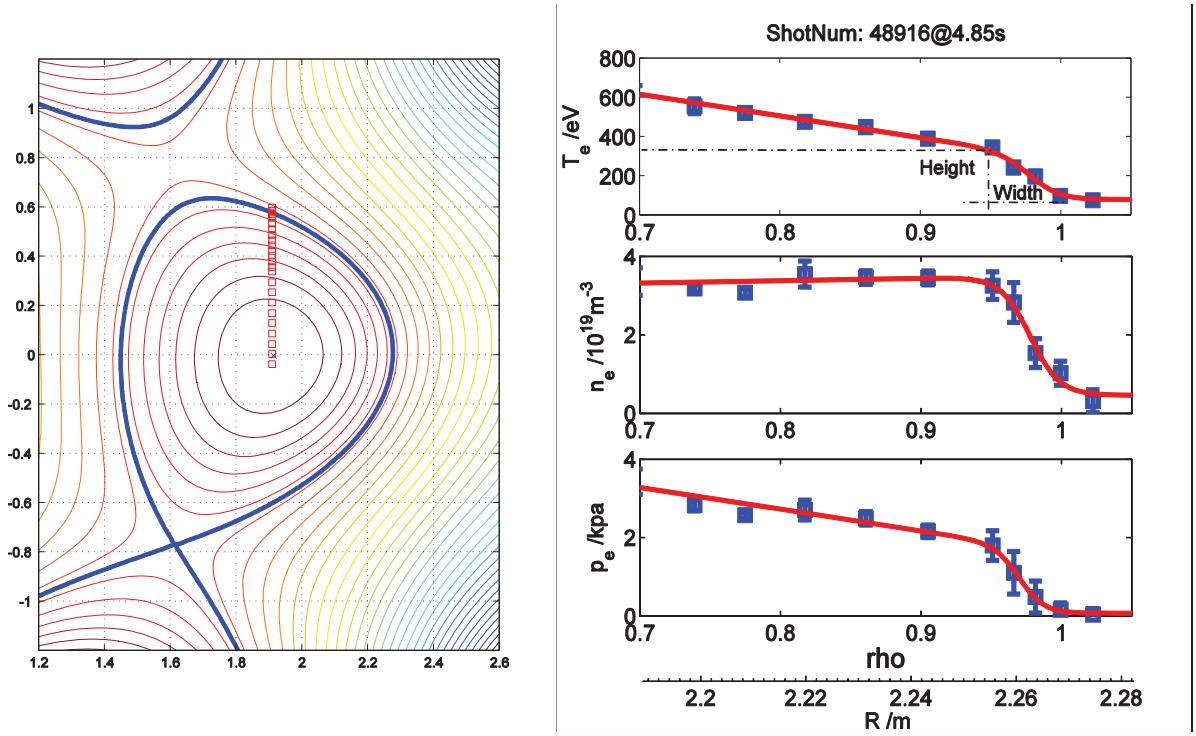

Figure 3. (*a*) Distribution of the measured points of the EAST TS diagnostic; (*b*) The Mthan function is used to fit the pedestal profile.

make all the data from different machines comparable, it is important to map R and z to normalized poloidal flux coordinates. In this paper, the normalized coordinates $\rho = \frac{1}{a}\sqrt{\frac{\Phi}{\pi B_0}}$ are defined as those given by DIII-D and the flux coordinates come from the results of the EAST EFIT calculation. Generally, the equilibrium needs reconstruction [13], and, sometimes, the TS data have to have a shift with respect to the separatrix position. In order to make up for limited measured points of the edge diagnostics, a fit function is necessary, in this paper, an Mthan function:

$$f(z) = c_1 \frac{(1 + c_3 * z)\exp(z) - \exp(-z)}{\exp(z) - \exp(-z)} + c_3,$$

with $z = \frac{2(c_4 - x)}{c_5}$, developed by Groebner [14], is involved to smooth the edge measurement, where c_5 means the width of the pedestal and $c_1 + c_3$ means the height of pedestal. Figure 3(*b*) gives a typical ELMy H-mode T_e, n_e, and electron pressure (p_e) profiles measured by the recent EAST Thomson system, and all the data are mapped on the normalized coordinates for pedestal research.

4. Characteristics of the EAST pedestal

The edge pedestal parameters are important for plasma performance as they determine the boundary conditions of the core plasma and also influence the energy confinement in tokamak power plants. The type I ELMy H-mode is the usual regime, with giant ELMs and large power loads on PFCs. By contrast, the type III ELMy H-modes have larger ELM frequency

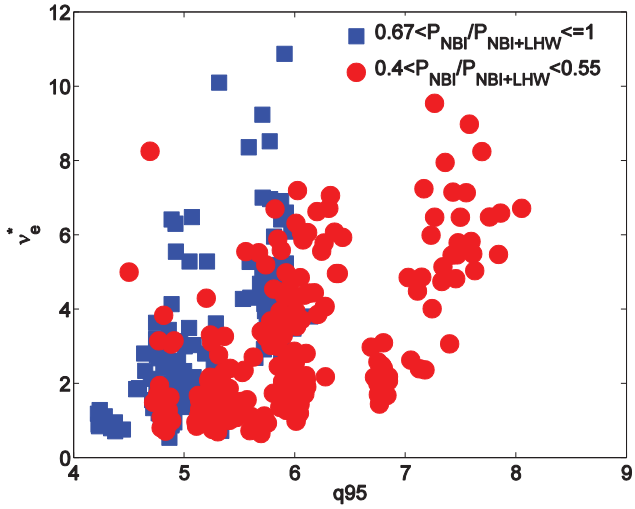

Figure 4. The collisionality of the pedestal and q_{95} of the EAST higher RNT and lower RNT discharges. $I_p = 400$–500 kA, $B_t = 2.3$ T, $\langle n_e \rangle = 2$–5.5×10^{19} m^{-3}, $P_{total} = 3.1$–4.5 MW, triangularity $= 0.4$–0.45, elongation $= 1.6$–1.7, LSN.

and smaller energy loss than type I ELMy H-modes. Due to reduced energy confinement and less experiment data, the type III ELMs regime has been researched less than type I ELMy H-modes. However, type III ELMs are believed to be beneficial to reducing the core transport; type III ELMs are therefore important for choosing a regime for ITER.

On EAST, as discussed above, based on LHW, both regular and irregular ELMs are observed for high power injection with different RNTs. Regular ELM (like type I ELMs) H-modes with higher RNT usually appear in the lower q_{95} region ($4 < q_{95} < 6$),

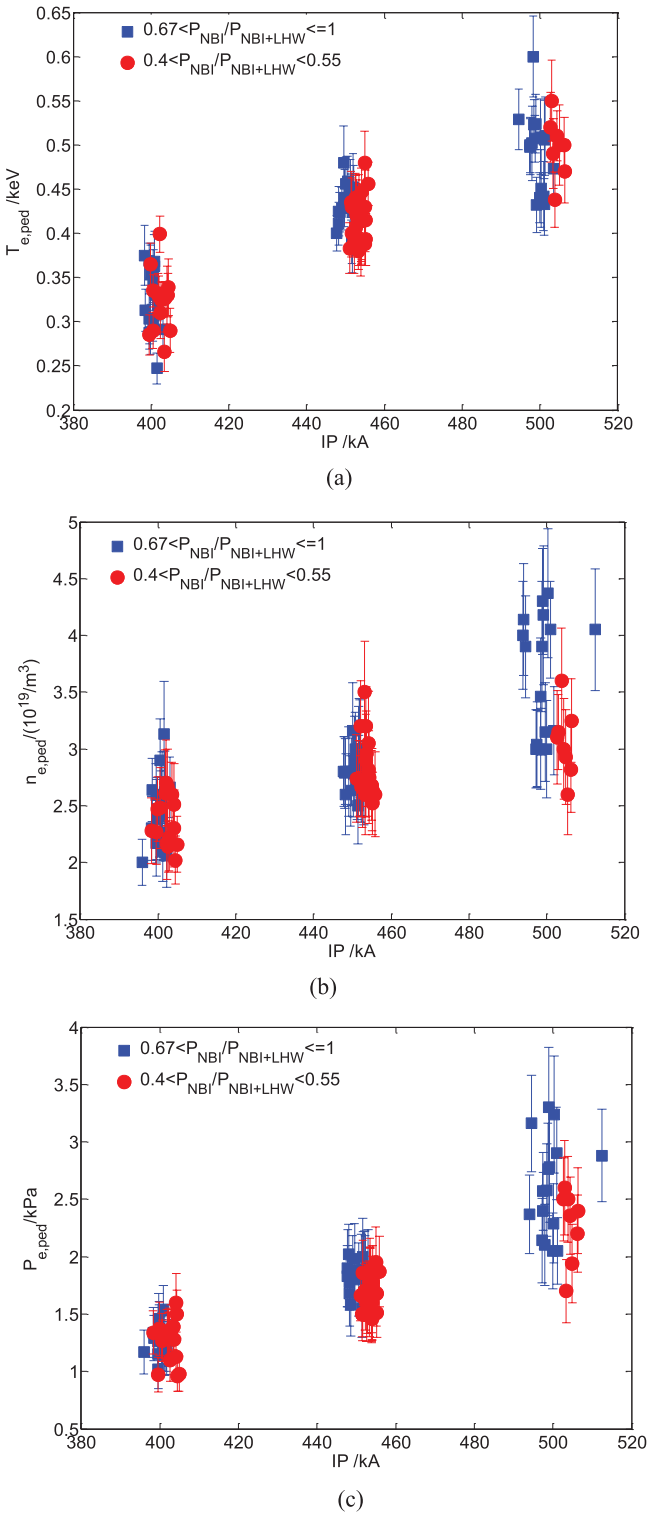

Figure 5. Dependence of the pedestal height of pedestal temperature (*a*), pedestal density (*b*) and pedestal pressure (*c*) on plasma current, $\langle n_e \rangle = 3.3\text{–}3.5 \times 10^{19}$ m^{-3}, $B_t = 2.3$ T, triangularity = 0.4–0.45, elongation = 1.6–1.7, LSN.

while irregular ELMs (like type III ELMs) with lower RNT usually appear in the higher q_{95} region ($5 < q_{95} < 8$), and the collisionality of both type of ELMy modes can be found in a wide range of 1–9 (figure 4). υ_e^* is defined as the ion–electron collision frequency normalized to the bounce frequency as [15]

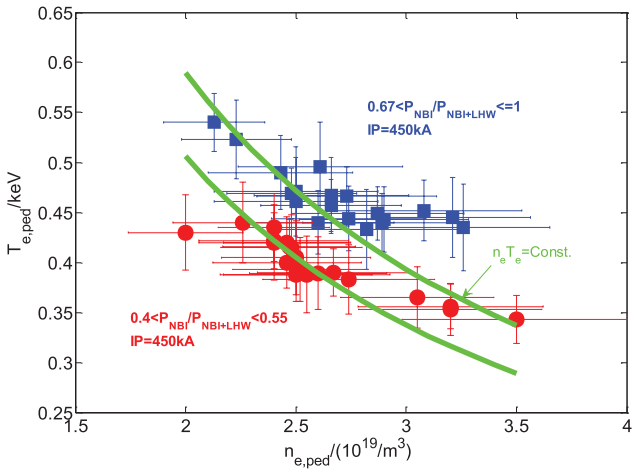

Figure 6. Pedestal n_e–T_e diagram for higher RNT and lower RNT discharges compared with constant pressure, $B_t = 2.3$T, $P_{total} =$ 3.9–4.1 MW, triangularity = 0.4–0.45, elongation = 1.6–1.7, LSN.

$$\upsilon_e^* = 6.930 \times 10^{-5} Z^2 \frac{q_{95} R_0 \ln \Lambda n_{e,ped}[10^{19}\,\mathrm{m}^{-3}]}{\varepsilon^{1.5}(T_{e,ped}\,(\mathrm{keV}))^2}$$

where ε is the inverse aspect ratio, $\ln \Lambda = 15.2 - 0.5 \ln(n_e\,(10^{20}\,\mathrm{m}^{-3})) + \ln(T_e\,(\mathrm{keV}))$, and assuming that in the pedestal region all the ions are deuterium.

The database involved in the report focuses on the above two types of discharge. About 500 individual measurements are selected in the pre-ELM time window of 50 shots with different plasma parameters. The main plasma parameters selected in the database are as follows: $I_p = 400\text{–}500$ kA, $B_t = 1.8$ T–2.3 T, $\langle n_e \rangle = 2\text{–}5.5 \times 10^{19}$ m^{-3}, $P_{total} = 3.1\text{–}4.5$ MW, triangularity = 0.4–0.45, elongation = 1.6–1.7, LSN.

In the following, three pedestal characteristics, height, width, and gradient of the higher RNT and lower RNT H-modes, observed on EAST discharges are discussed, and the relationship of these characteristics with plasma parameters are also described in detail.

4.1. Pedestal height

For the stiffness in the temperature profiles, the energy confinement and the fusion gain are strongly affected by the pedestal temperature, and expecting a high confinement enhancement achieved at a high density, the improved pedestal pressure then becomes essentially important for H-mode research.

On EAST, the top values of pedestal temperature are in the range 250 eV–550eV for higher RNT and lower RNT ELMy H-modes, and both regimes have similar $T_{e,ped}$ at the same plasma current (figure 5(*a*)). For the different RNTs, $T_{e,ped}$ increases nearly linearly with the plasma current, but when I_p is close to 450 kA, $n_{e,ped}$ ceases to increase in the lower RNT scenario, while $n_{e,ped}$ still increases linearly in the higher RNT scenario, so the $p_{e,ped}$ in the higher RNT regime increases faster than that of the lower RNT regime when the plasma current is larger than 450 kA. These results show that the large plasma current favors achieving high values of pedestal height, and these dependences are consistent with the expression of energy confinement time $\tau_E^{ITER98} = 0.094 I^{0.97} B^{0.08} P^{-0.63} n^{0.41} A^{0.2} R^{1.93} \varepsilon^{0.23} \kappa^{0.67} s$.

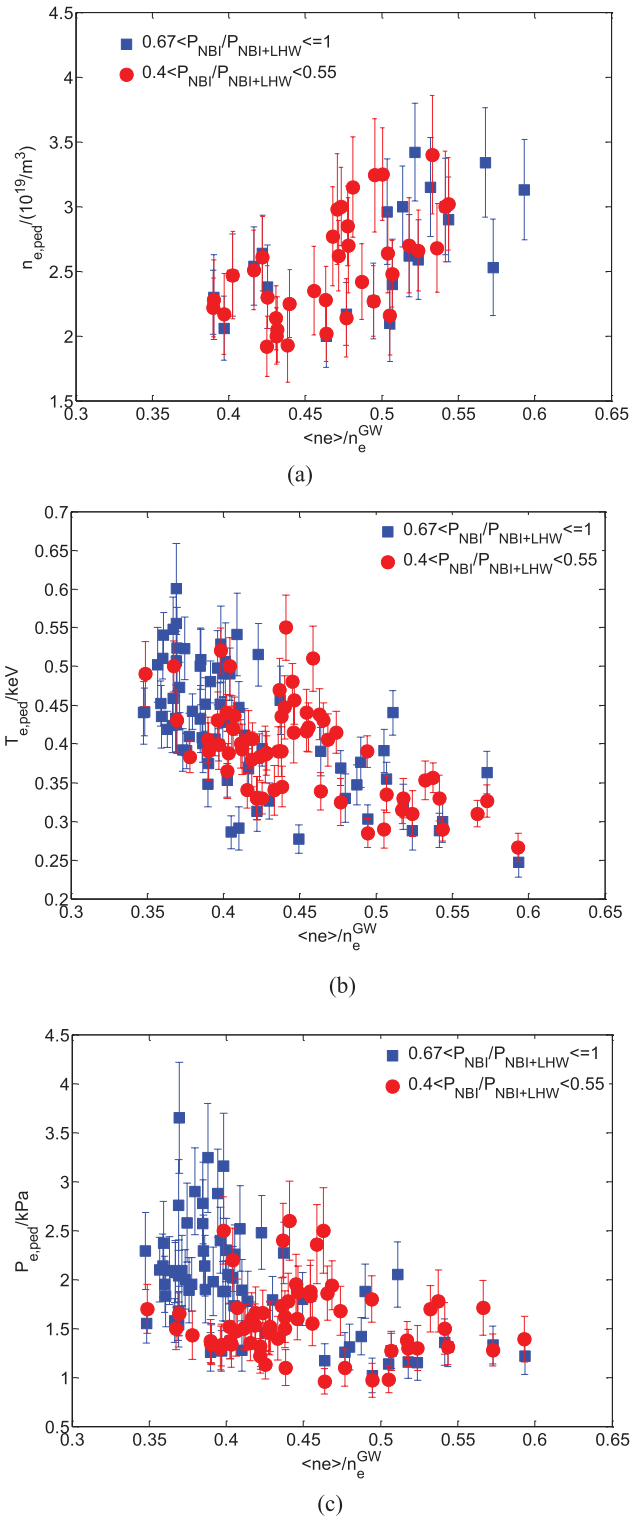

Figure 7. Dependence of pedestal height of pedestal density (*a*), pedestal temperature (*b*) and pedestal pressure (*c*) on plasma density normalized by Greenwald density limit, $I_p = 400$–500 kA, $B_t = 2.3$ T, $P_{total} = 3.1$–4.5 MW, triangularity $= 0.4$–0.45, elongation $=$ 1.6–1.7, LSN.

Furthermore, the higher RNT H-mode has higher $n_{e,ped}$ and $p_{e,ped}$ than the lower RNT H-modes, and the H-factor of the higher RNT H-mode is about 10% larger than that of the lower RNT H-modes, so it is believed that the higher RNT H-mode has better performance.

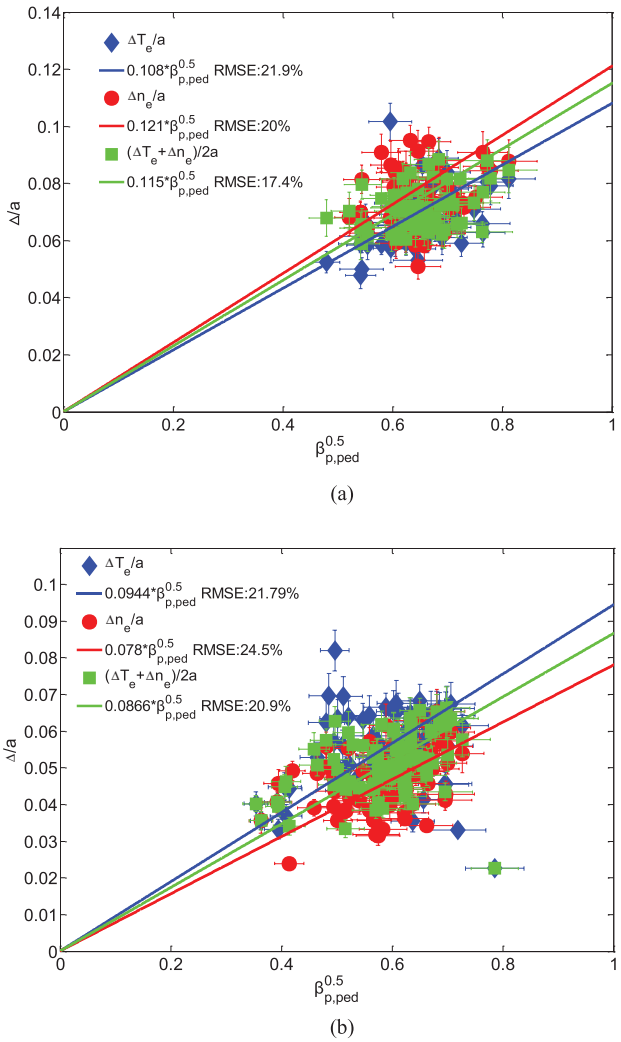

Figure 8. Dependence of the pedestal width in real space coordinates on $\beta^{0.5}_{p,ped}$ for higher RNT H-mode discharges (*a*) and lower RNT H-mode discharges (*b*). $I_p = 400$–500 kA, $B_t = 2.3$ T, $\langle n_e \rangle = 2$–5.5×10^{19} m^{-3}, $P_{total} = 3.1$–4.5 MW, triangularity $= 0.4$–0.45, elongation $= 1.6$–1.7, LSN.

In fact, if all the parameters of the plasma are the same, when the pedestal density increases, the pedestal temperature decreases; the electron pressure is a constant value (figure 6). Figure 7(*a*) shows that for higher RNT or lower RNT, when the line average density increases, the pedestal density increases at the same time, and $T_{e,ped}$ and $p_{e,ped}$ decrease with increasing $\langle n_e \rangle / n^{GW}$. However, for lower density, it seems easy to achieve the regular ELMs H-mode with higher temperature and pedestal pressure (figures 7(*b*) and (*c*)). Experiments also show that the pedestal pressure height has no relation to the toroidal field.

4.2. Pedestal width

The H-mode transport barrier is believed to be the result of the suppression of turbulence at the plasma edge, and it is suspected that the gradient of the pedestal is limited by the edge instability of the ideal ballooning mode; the extension of the steep region then become essential to determining the height of the pedestal [16]. Although several theoretical models have

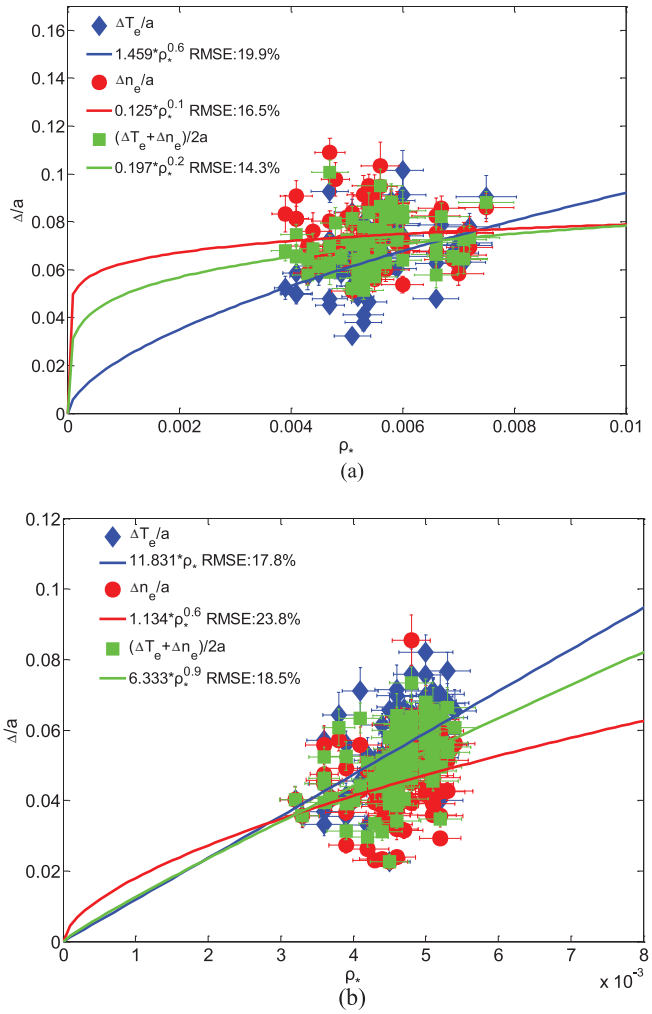

Figure 9. Dependence of the pedestal width in real space coordinates on ρ^* for higher RNT H-mode discharges (a) and lower RNT H-mode discharges (b). $I_p = 400$–500 kA, $B_t = 2.3$ T, $\langle n_e \rangle = 2$–5.5×10^{19} m^{-3}, $P_{total} = 3.1$–4.5 MW, triangularity $= 0.4$–0.45, elongation $= 1.6$–1.7, LSN.

been proposed to explain the width of the pedestal [17–19], in this paper only two predictions are examined to find a best description of the EAST pedestal width. The edge transport barrier width of EAST measured by TS is normalized on the outer midplane of the flux surface. From figure 8 we find that the temperature pedestal width (ΔT_e) of the higher RNT H-mode is about $0.06a$ (a is the minor radius), and approximately equals the width of lower RNTs, while the density pedestal width (Δn_e) of the higher RNT H-mode is about $0.07a$, which is 50% larger than the width of the lower RNTs. So the mean pedestal width ($\Delta T_e + \Delta n_e$)/2 of larger RNT H-modes is almost 25% wider than that of the lower RNT H-mode.

However, the theory of kinetic ballooning modes predicts a $\beta_{p,ped}^{0.5}$ dependence of the pedestal width in Ψ_N [20]. A correlation with the square root of the poloidal pedestal beta $\beta_{p,ped}^{0.5} \propto \beta_{p,ped}^{0.5} B_p^{-1}$ was observed in DIII-D for the electron pressure pedestal width for real space coordinates [21], and the mean pedestal ($\Delta T_e + \Delta n_e$)/2 was also found to fit to $\beta_{p,ped}^{0.5}$ in normalized poloidal flux coordinated Ψ_N, as shown in [22, 23]. For AUG the mean pedestal width showed a linear correlation with $\beta_{p,ped}^{0.5}$ in Ψ_N but no correlation in real space [24]. JT-60U also found a dependence of the ion temperature width on $\beta_{p,ped}^{0.5}$ in real space [25]. On EAST, we found that the mean pedestal width shows good correlation with $\beta_{p,ped}^{0.5}$ in real space (figure 8(a)) for both higher RNT and lower RNT H-modes. Considering the coefficient of DIII-D correlation, the EAST pedestal width of the higher RNT H-mode is almost 50% wider than that of DIII-D; it is suspected that a lithium coating helps to enlarge the width of the pedestal, as reported in NSTX and DIII-D [26, 27]

In Shaing's model, the source of the $\mathbf{E_R} \times \mathbf{B}$ shearing is limited to the region of ion orbit loss across the plasma boundary and the pedestal width was described as $\delta \propto \rho_p^i$ [16, 28], so a $\rho^* \propto T_I^{0.5} M^{0.5} a^{-1} B_t^{-1}$ dependence was discussed [21, 24, 25, 29]. In JT-60U, the dependence of the ion temperature width on ρ_*^ξ was found to be less than $\xi = 0.2$ [25], while in DIII-D the dependence was found when the variation of mass number was used to test a ρ^* dependence of the mean pedestal width in flux coordinates [23]. More recently several experiments were performed with variation of machine size between DIII-D and JET, which showed that there were no consistent correlations with ρ^* for electron temperature and electron density pedestal width in real space [24]. We also tried to use different ξ to find correlations with ρ^*, (Figure 9) but there seems to be no obvious best fit when ξ changes in a wide range. Considering the limited operation region, for the time being, we cannot get conclusive correlation for ρ^*.

4.3. Pedestal gradients

It is believed that ELMs limit the pedestal pressure gradient, and edge transport may directly limit the top values of the pedestal pressure and temperature, so the pressure gradient is often regarded in connection with the MHD stability of ELMs and different aspects in pedestal physics. However, the bootstrap current depends on temperature and density gradients; the gradients of temperature and density are individually important independent of pressure [28–30]. In figure 10, the features of temperature, density and pressure gradients are illustrated. Although the scatter is quite large, all gradients appear to be strongly correlated with the pedestal top values, and both higher RNT and lower RNT H-modes have a similar trend. In particular, both higher RNT and lower RNT H-mode temperature gradients scale linearly with the pedestal top temperature and give $T_e/\nabla T_e \sim 2$ cm regardless of other plasma parameters, which is the same as the AUG, DIII-D and JET results [31]. Furthermore, in this report, $n_e/\nabla n_e$ and $p_e/\nabla p_e$ are also equal to ~2 cm, whether for the higher RNT H-mode or the lower RNT H-mode.

5. Summary and discussion

With the increase of the power of the heating system of EAST, type I-like ELM and type III-like ELM H-modes have been achieved with NBI or/and LHW heating. In this paper, the different frequency dependency on RNT is introduced. Using the recently developed TS diagnostic, the pedestal structure of both ELM H-modes can be clearly given with Mthan function fitting. From the scanning, for higher RNT or lower RNT

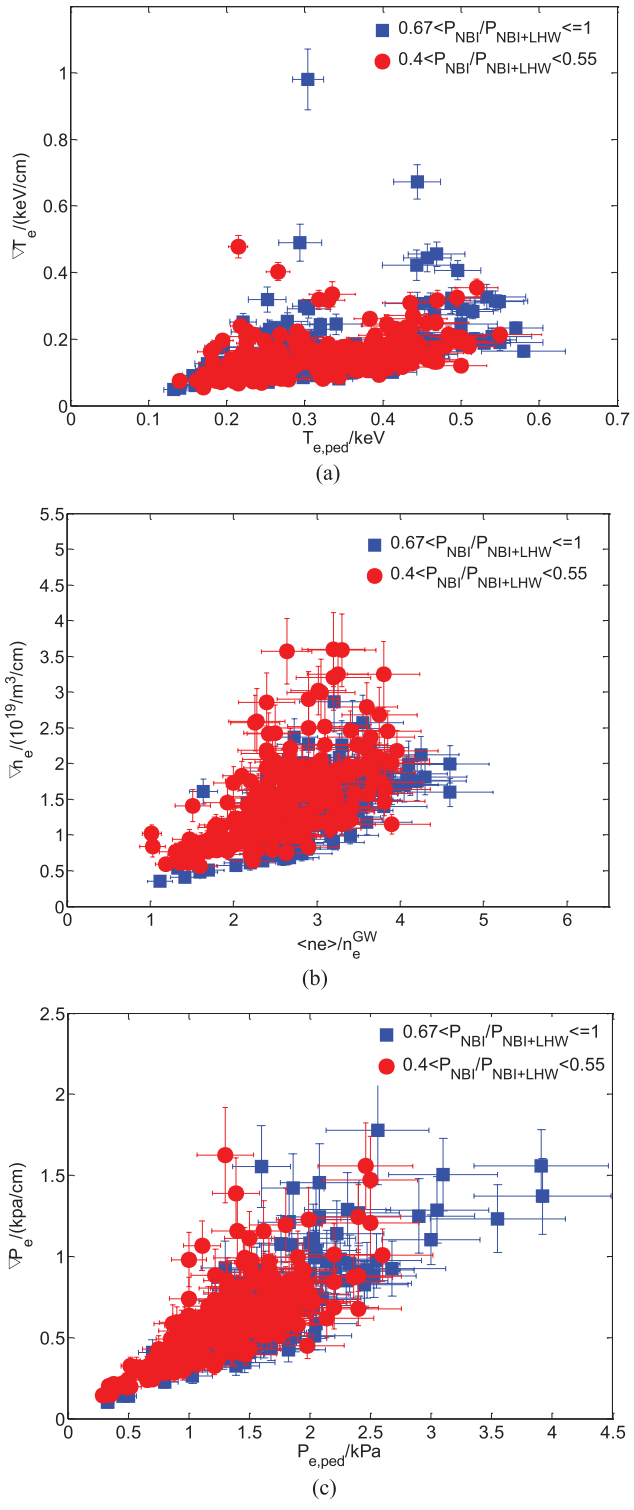

Figure 10. Dependence of the temperature gradient on pedestal temperature (*a*), density gradient on pedestal density (*b*) and pressure gradient on pedestal pressure (*c*) for higher RNT H-modes and lower RNT H-modes. $I_p = 400$–500 kA, $B_t = 2.3$ T, $\langle n_e \rangle = 2$–5.5×10^{19} m^{-3}, $P_{total} = 3.1$–4.5 MW, triangularity $= 0.4$–0.45, elongation $= 1.6$–1.7, LSN.

H-modes, the electron pressure is a constant value, however, for the same plasma parameters and input power, the higher RNT has a higher height of electron pressure. The mean pedestal width $(\Delta T_e + \Delta n_e)/2$ of the higher RNT H-mode is almost 25% wider than the lower RNT H-mode. For both regimes, the mean pedestal width shows good correlation with $\beta_{p,ped}^{0.5}$ in real space, and the EAST pedestal appears 50% wider than that of DIII-D without lithium coating. On EAST, $T_e/\nabla T_e$, $n_e/\nabla n_e$ and $p_e/\nabla p_e$ are all about 2 cm, and the conclusion of $T_e/\nabla T_e$ is the same as the results achieved for AUG, DIII-D and JET [31].

The pedestal data are strongly limited by diagnostic capabilities; in this paper, the spatial and data points across the pedestal region are not sufficient to derive a very accurate pedestal structure, so a high spatial edge TS diagnostic is needed for EAST. On the other hand, although details of the error bars for the data used in this paper are shown, and fitting including the error and possible uncertainties are taken into account, a statistical examination should be carried out in the future.

Acknowledgments

This work is supported by the National Natural Science Foundation of China under Grant No. 11275233, the National Magnetic Confinement Fusion Science Program of China Grant No. 2013GB112003, 2013GB106003B, 2015GB103001, and 2015GB101002, and is partly supported by the PRC-US Fusion Cooperation Program.

References

[1] Wagner F. *et al* 1982 *Phys. Rev. Lett.* **49** 1408
[2] Gohil P. *et al* 1988 *Phys. Rev. Lett.* **61** 1603
[3] Ozeki T. *et al* 1990 *Nucl. Fusion* **30** 1425
[4] Zohm H. *et al* 1995 *Nucl. Fusion* **35** 543
[5] Wade M.R. *et al* 2004 *Phys. Rev. Lett.* **92** 235005
[6] Doyle E.J. *et al* 2002 *Nucl. Fusion* **42** 333
[7] Wang L. *et al* 2013 *Nucl. Fusion* **53** 073028
[8] Li J. *et al* 2013 *Nat. Phys.* **9** 817
[9] Lian Y. *et al* 2013 *Phys. Rev. Lett.* **110** 235002
[10] Wang J. *et al* 2015 *Fusion Eng. Des.* **101** 56
[11] Zang Q. *et al* 2011 *Rev. Sci. Instrum.* **82** 063502
[12] Zang Q. *et al* 2013 *Rev. Sci. Instrum.* **84** 093504
[13] Li G.Q. *et al* 2013 *Plasma Phys. Control. Fusion* **55** 125008
[14] Groebner R.J. *et al* 2001 *Nucl. Fusion* **41** 1789
[15] Sauter O. *et al* 1999 *Phys. Plasmas* **6** 2834
[16] Sugihara M. *et al* 2000 *Nucl. Fusion* **39** 1743
[17] Shaing K.C. *et al* 1989 *Phys. Rev. Lett.* **63** 2369
[18] Hinton F.L. *et al* 1993 *Phys. Fluids* B **5** 1281
[19] Kotschenreuther M. *et al* 1997 *Proc. 16th Int. Conf. on Fusion Energy (Montreal, 1996)* vol 2 (Vienna: IAEA) p 371
[20] Snyder P.B. *et al* 2009 *Nucl. Fusion* **49** 085035
[21] Osborne T. *et al* 1999 *J. Nucl. Mater.* **266** 131
[22] Snyder P.B. *et al* 2009 *Phys. Plasmas* **16** 056118
[23] Groebner R.J. *et al* 2009 *Nucl. Fusion* **49** 085037
[24] Beurskens M.N.A. *et al* 2011 *Phys. Plasmas* **18** 056120
[25] Urano H. *et al* 2008 *Nucl. Fusion* **48** 045008
[26] Osborne T.H. 2015 *Nucl. Fusion* **55** 063018
[27] Maingi R. *et al* 2011 *Phys. Plasmas* **18** 056118
[28] Shaing K.C. *et al* 1992 *Phys. Fluids* B **4** 290
[29] Groebner R.J. *et al* 1998 *Phys. Plasmas* **5** 1800
[30] Snyder P.B. *et al* 2002 *Phys. Plasmas* **9** 2037
[31] Schneider P.A. 2012 Characterization and scaling of the tokamak edge transport barrier, Ludwig Maximilians Universität München and Max Planck Institut für Plasmaphysik *PhD Thesis* 99